ELSEVIER

Thermochimica Acta 255 (1995) 49–61

thermochimica acta

Equilibrium phase diagram of the water–sucrose–NaCl system

E.Yu. Shalaev [1], F. Franks *

Pafra Ltd., Bipreservation Division, 150 Science Park, Cambridge CB4 4GG, UK

Received 13 June 1994; accepted 6 November 1994

Abstract

The solid–liquid equilibrium phase relationships in the ternary system water–NaCl–sucrose have been established with the aid of DSC measurements in the water-rich region and literature data. The phase coexistence conditions are represented in a plane projection of the three-dimensional phase diagram. The existence of the following stoichiometric hydrates has been taken into account: $NaCl \cdot 2H_2O$, $C_{12}H_{22}O_{11} \cdot 2.5H_2O$, $C_{12}H_{22}O_{11} \cdot 3.5H_2O$ and $NaCl \cdot C_{12}H_{22}O_{11} \cdot 2H_2O$. The coordinates of the binary and ternary eutectic and peritectic points are established with varying degrees of confidence.

Keywords: DSC; Hydrate; Phase diagram; SLE; Stoichiometry; Ternary system

List of symbols

$T_1, T_2, \ldots, T_n$	Transition temperatures (identified as endothermic processes in DSC heating scans)
L	unsaturated solution
$\langle\rangle$	crystalline phase
$e_1, e_2, \ldots, e_n$	binary eutectic points
E_1, E_2	ternary eutectic points
$p_1, p_2, \ldots, p_n$	binary peritectic points
P	ternary peritectic point
I	$C_{12}H_{22}O_{11} \cdot 3.5H_2O$(s)
II	$C_{12}H_{22}O_{11} \cdot 2.5H_2O$(s)

* Corresponding author.
[1] Present address: School of Pharmacy, University of Wisconsin, Madison, WI, USA.

SSDI 0040-6031(94)02180-5

III	$NaCl \cdot 2H_2O(s)$
IV	$NaCl \cdot C_{12}H_{22}O_{11} \cdot 2H_2O(s)$
k, l, m	polynomial fitting coefficients in Eq. (1)
R	sucrose/NaCl mass ratio; see Eq. (2)
x	water/NaCl mass ratio; see Eq. (3)

1. Introduction

The physical properties of complex aqueous systems, and especially heterogeneous equilibria between liquid and solid phases, are fundamental to an understanding of natural processes, such as freezing, desiccation and geochemical phenomena at elevated temperatures. They are also basic to several technologies in diverse branches of industry (biotechnology, pharmaceutics, food processing, ceramics, metallurgy). The description of heterogeneous phase equilibria by means of phase diagrams was developed by Gibbs; traditional investigations relied on solubility measurements and determinations of freezing point depressions. Data reported several decades ago in the "old literature" are probably as reliable as those obtained by "modern" methods. Unfortunately much of the "old" information is no longer referred to nowadays. Thermal analytical and diffraction methods, developed more recently, have made possible the direct recording of solid–solid and solid–liquid transitions; these methods are not performed under equilibrium conditions so the results need careful and expert interpretation.

Multicomponent aqueous mixtures, especially those containing carbohydrates, are of great ecological and technological interest. They present experimental and interpretative problems because only a portion of the composition–temperature surface can be explored; in the carbohydrate-rich region crystallisation is usually very slow or does not occur at all in real time. Instead, the mixtures undergo glass transitions [1]. This study extends our previous investigations into the phase behaviour of ternary aqueous systems by thermal analysis methods [1–3]. It was confined to those regions of the composition–temperature surface in which equilibrium phase boundaries can be measured by thermal scanning methods. A study of the complete state diagram, including amorphous solid solutions, will be reported later.

2. Materials and methods

Pure, microcrystalline sucrose was a gift from Tate and Lyle Ltd. NaCl was of BDH Laboratory grade (99.9%). The crystalline chemicals were used without further purification. Distilled water was used for all experimental work.

The modified Perkin-Elmer DSC-2 instrument used in this work was fitted with Auto-scanning Zero and sub-ambient temperature accessories. The DARES data handling system was used for monitoring and processing heat flow–time curves [4]. The scanning rate for cooling and heating runs was 5 K min^{-1}. Low temperature limits were in the range 210–220 K. DSC heating curves were recorded from 215 to 230 K. Thermal cycling programmes (cooling–heating up to 240–245 K–cooling–heating) and annealing at 245 K during one hour were used in some cases.

The compositions of the mixtures examined are represented in Fig. 1. The method of polythermic isoplethal sections, developed by Petrov [5], was used to examine the ternary phase diagram. The solutions were prepared in 10 ml tubes, using a balance of 0.1 mg precision. Solutions belonging to sections 1–3 (Fig. 1) were prepared by the addition of NaCl to binary aqueous sucrose solutions, with sucrose concentrations of 10.0 (section 1), 20.0 (section 2) and 29.8% w/w (section 3). Solutions close to the NaCl saturation solubility ("hyper-eutectic" compositions) were prepared by the addition of the calculated amount of sucrose to the aqueous sodium chloride solutions. Each solution was transferred to an aluminium DSC pan and sealed hermetically. Sample masses were 0.6–1.4 mg in most cases. For "hyper-eutectic" compositions, sample masses were 6–12 mg, because of the low intensity of the thermal signal associated with the incongruent melting of $NaCl \cdot 2H_2O$. Transition temperatures were determined as the peak temperatures on the DSC curves. The correspondence between the temperatures of the melting peaks and the liquidus temperatures was checked for four binary sucrose and NaCl solutions of varying concentrations; the correlation was satisfactory for sample masses below 1.5 mg. The estimated error in the transition temperatures was 1 K and included the DSC scan reproducibility for successive measurements, together with calibration uncertainties.

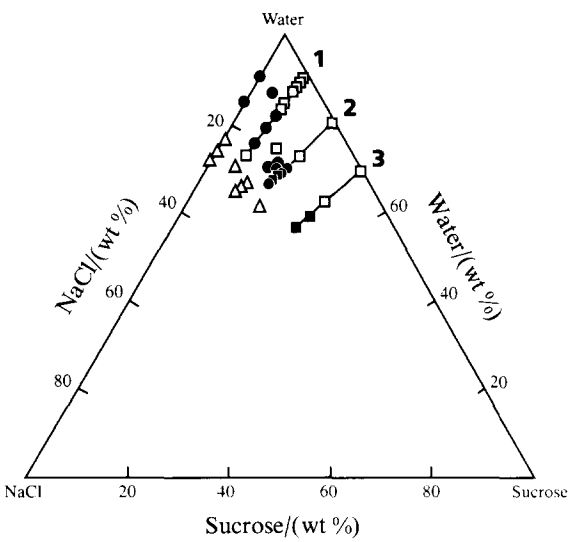

Fig. 1. Composition triangle for the ternary system water–NaCl–sucrose: □, solutions that exhibited one exotherm during cooling and one endotherm during heating; ●, solutions that exhibited two endotherms during heating; ■, no thermal effects observed during either cooling or heating; △, "hyper-eutectic" solutions. For the compositions of sections 1–3 see text.

Table 1
Coordinates of invariant points in the binary systems water–sucrose and water–NaCl

Equilibrium [a]	Composition/ %Water	T/K	System	Ref.
Eutectic L/ice + I	44.1	263.3	H_2O–sucrose	[3]
Peritectic L + II/I	36.3	274.0		[3]
Peritectic L + Suc/II	35.3	275.8		[3]
Eutectic L/ice + III	76.89	252.15	H_2O–NaCl	[6]
Peritectic L + Sod/II	73.71	273.28		[6]

[a] Suc, sucrose; Sod, NaCl; roman numerals refer to stoichiometric hydrates (see List of symbols).

3. Results and discussion

3.1. Binary systems

3.1.1. Water–NaCl

Water and NaCl form a simple eutectic system with an incongruently melting crystallohydrate $NaCl \cdot 2H_2O$ (III). Coordinates of the invariant points are included in Table 1. Characteristic DSC heating scans for "hyper-eutectic" solutions are shown in Fig. 2. The exact shapes of the DSC curves depend on the thermal history of the samples. In the case of cooling from 360 K to 210 K followed by heating, eutectic melting (not shown) and one weak endotherm were observed (scan 1). An additional peak was observed for samples which were held at room temperature for

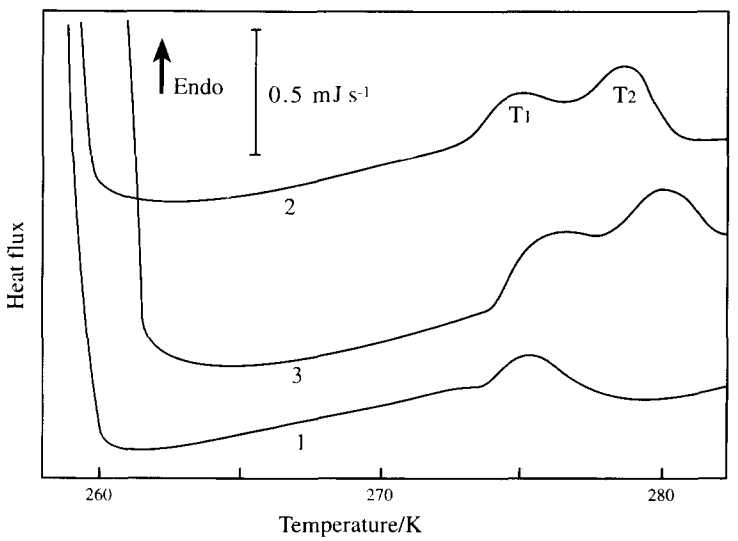

Fig. 2. DSC heating scans for a 26.83% binary NaCl–water solution. Heating rate, 5 K min^{-1}; sample masses, (curve 1) 7.518 mg; (curve 2) 9.937 mg; (curve 3) 8.131 mg. Thermal histories: (curve 1) 360 K–210 K–heating; (curve 2) 300 K–210 K–heating; (curve 3) 300 K–210 K–245 K–210 K–heating.

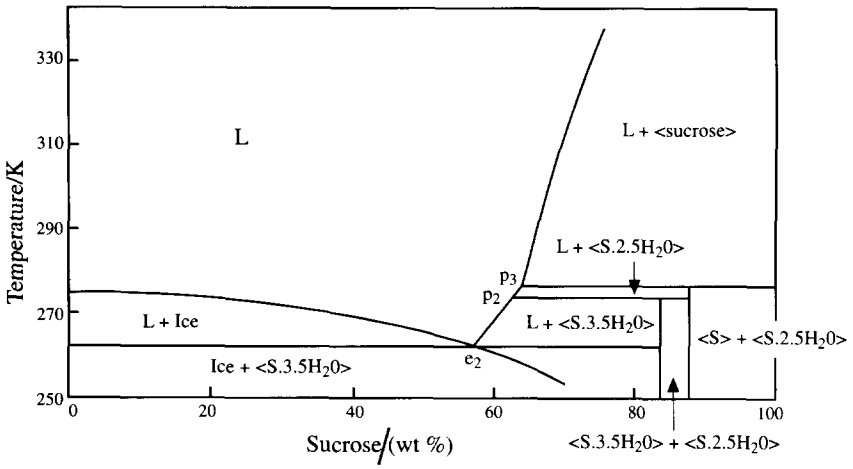

Fig. 3. Phase diagram of the water–sucrose system, constructed from data in Refs. [3], [7] and G. Vavrinecz, Z. Zuckerind., 12 (1962) 481–487.

5–10 min before being cooled (scan 2) or were subjected to thermal cycling (scan 3) (cooling–heating to 245 K–cooling). We consider that the weak endotherm T_1 corresponds to the invariant peritectic transition of $NaCl \cdot 2H_2O$. The origin of the "high"-temperature peak T_2 is obscure. It cannot be the thermal effect of NaCl dissolution because it appears well below the temperature of NaCl solubility for this composition. It may possibly be assigned to the melting of $NaCl \cdot nH_2O$ (where $n < 2$); however, there is no reported evidence for the existence of a crystal hydrate other than the well known dihydrate.

3.1.2. Water–sucrose

According to Ref. [7], eight hydrates can exist in water–sucrose systems. The existence of only two such stoichiometric hydrates has been confirmed by X-ray diffraction; their compositions, namely $C_{12}H_{22}O_{11} \cdot 2.5H_2O$ (II) and $C_{12}H_{22}O_{11} \cdot 3.5H_2O$ (I), were confirmed by chemical analysis. The equilibrium phase diagram of the system water–sucrose, taking into account the two hydrates, was constructed by Kanev et al. [3] and is shown in Fig. 3. Table 1 gives the calculated coordinates of the invariant points. In practice, however, only ice crystallises when sucrose solutions are cooled. No eutectic mixtures crystallise within the timescale of DSC experiments.

3.1.3. Sucrose–NaCl

No quantitative information exists on the phase diagram of the (anhydrous) binary system, although the crystallisation of NaCl from its solution in amorphous sucrose has been observed by electron microscopy [8].

3.2. The ternary system

The solubility relationships for the ternary system have been reported for the temperature range 293.15–333.15 K [9,10]. The existence of the ternary compound $C_{12}H_{22}O_{11} \cdot NaCl \cdot 2H_2O$ (IV) has been confirmed by X-ray diffraction, chemical analysis of the separated crystals, and the refractive index [9]. Solubility isotherms and points on the projections of the lines of the monovariant equilibria (secondary crystallisation of NaCl + IV and sucrose + IV) are shown in Fig. 4.

The corresponding DSC heating curves are collected in Figs. 5 and 6. Fig. 5 shows DSC scans for compositions designated by □, ● and ■ in Fig. 1. Curve 3 in Fig. 5 is typical for sucrose-rich mixtures. One exothermic effect was observed during cooling and one endothermic transition during heating. For NaCl-rich solutions two distinct types of behaviour were observed. In one case no transitions occurred during cooling or heating. After thermal cycling (heating to 245 K–cooling–heating) one broad melting endotherm appeared on the DSC scan (curve 1). In the second case, ice crystallisation took place during cooling. One shallow exotherm and two endotherms were observed in the DSC heating curves (curve 2). The exotherm may be assigned to the secondary water of crystallisation + $NaCl \cdot 2H_2O$. Endothermic peaks are due to the melting of ice (T_4) and the eutectic melting of ice + $NaCl \cdot 2H_2O$ (T_3). Thermocycling did not affect either T_4 or T_3.

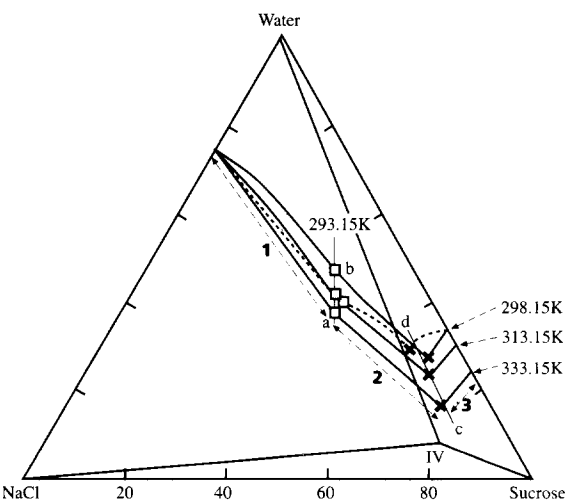

Fig. 4. Solubility isotherms for the water–NaCl–sucrose system [8,9]: 1, NaCl; 2, IV; 3, sucrose, at the indicated temperatures. Broken lines are isotherms at 298.15 K from Ref. [9]; ab is the projection of the monovariant line of secondary crystallisation of NaCl + IV; cd is the projection of the monovariant line of the secondary crystallisation of sucrose + IV; □, points on the projection of the monovariant line of the secondary crystallisation of NaCl + IV; ×, points on the projection of the monovariant line of the secondary crystallisation of sucrose + $NaCl \cdot C_{12}H_{22}O_{11} \cdot 2H_2O$; IV, composition of the ternary compound $NaCl \cdot C_{12}H_{22}O_{11} \cdot 2H_2O$.

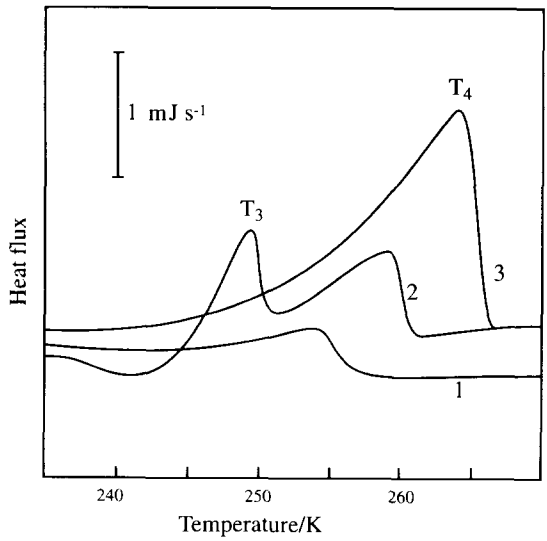

Fig. 5. Representative DSC heating curves for ternary solutions at a heating rate of 5 K min^{-1}: curve 1, 14.57% NaCl, 17.09% sucrose, 68.34% water, after 1–3 thermal cycles (sample mass = 0.678 mg); curve 2, 12.36% NaCl, 17.55% sucrose, 70.09% water (sample mass = 0.943 mg); curve 3, 8.32% NaCl, 18.36% sucrose, 73.32% water (sample mass = 1.537 mg). For interpretation see text.

Typical DSC curves for "hyper-eutectic" ternary solutions are shown in Fig. 6. The temperature of the T_1 effect decreased with repeated cooling–heating cycles of cooling–heating to 300 K–cooling. After two or three cycles, T_1 attained a constant value. The same value was registered for annealed samples. The temperatures attained after repeated cycling (cooling–heating to 300 K–cooling) or after annealing at 245 K for one hour were assigned to the equilibrium temperature of the incongruent melting of $NaCl \cdot 2H_2O$. There are other, minor, unidentified thermal effects above the peritectic temperature, analogous to those detected for the binary NaCl–water solutions; we neglected these effects in the construction of the equilibrium phase diagram.

3.2.1. Construction of the equilibrium ternary phase diagram

To determine the phase composition of a mixture with a given composition, at an arbitrary temperature, it is convenient to use the plane projection of the three-dimensional phase diagram. The general appearance of the projection of the ternary diagram with a ternary compound and with the incongruent melting of a binary crystal hydrate is shown in Fig. 7; here A is H_2O. Experimental data obtained in this work, combined with results from Refs. [9] and [10] permit (in principle) the construction of the following elements of the equilibrium phase diagram. (1) Bivariant equilibria (shown as surfaces): water liquidus, solubilities of NaCl, sucrose, and compound IV. (2) The following monovariant equilibrium surfaces: secondary crystallisations of NaCl + IV, sucrose + IV, ice + III, and the incongruent melting of III. (3) Invariant peritectic equilibrium $\langle III \rangle + L/\langle NaCl \rangle + \langle IV \rangle + L$.

(1) Bivariant equilibrium surfaces. These surfaces define the equilibria between one crystalline and one liquid phase, ⟨A⟩ + L/L. For such surfaces, a representation by isotherms in the composition triangle is most convenient.

For surfaces corresponding to the solubilities of NaCl, sucrose and IV, solubility isotherms, obtained from Refs. [9] and [10] are shown in Fig. 4. Points shown on the solubility isotherms were determined from Fig. 1 in Ref. [9].

For the water liquidus surface Fig. 8 was used to construct the isotherms. The experimental points were smoothed by a second-order least-squares polynomial with the aid of the easyPLOT software.

$$T_4 = k + lw + mw^2 \tag{1}$$

where T_4 is the liquidus temperature, w is the weight percentage of NaCl, and k, l, m are the polynomial coefficients (Table 2).

The compositions belonging to the isotherms were determined graphically at four selected temperatures (253.15, 258.15, 263.15 and 268.15 K) and the isotherms are marked on the composition triangle in Fig. 9 by broken lines 1–4.

(2) Monovariant equilibrium surfaces ⟨A⟩ + ⟨B⟩ + L/⟨A⟩ + L *and* ⟨B · xA⟩ + L/⟨B⟩ + L. These linear surfaces describe the phase composition of a material consisting of one liquid and two solid phases. The temperatures of the ⟨A⟩ + ⟨B⟩ + L/⟨A⟩ + L equilibrium are therefore independent of the concentration of component A but depend on the ratio B/C. Surfaces of the solubility and the

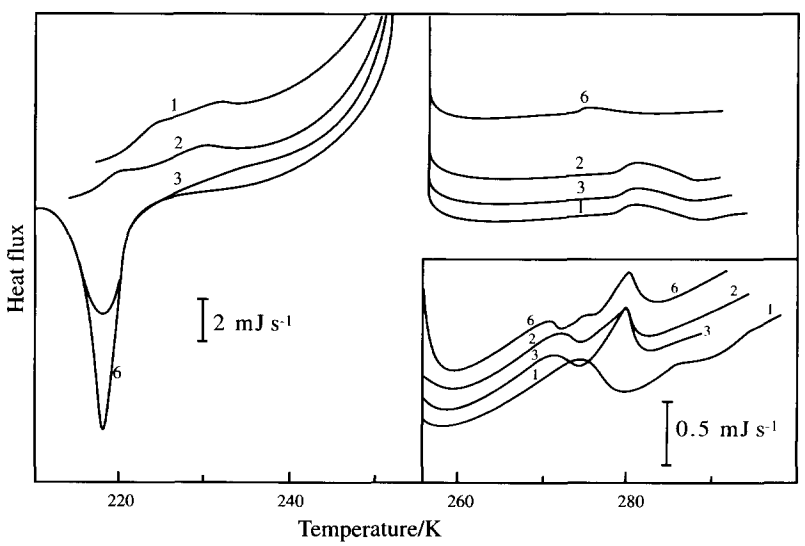

Fig. 6. DSC heating scans for the ternary solution containing 22.47% NaCl and 16.70% sucrose; heating and cooling rates were 5 K min^{-1}; sample mass = 10.706 mg. 1, 2, 3, 6 indicate the current number n of the cooling/heating cycle (360 K–210 K–300 K)$_n$–210 K–heating, ($1 \leq n \leq 6$). Inset: expanded sections of the DSC scans near the melting temperature of the peritectic mixture.

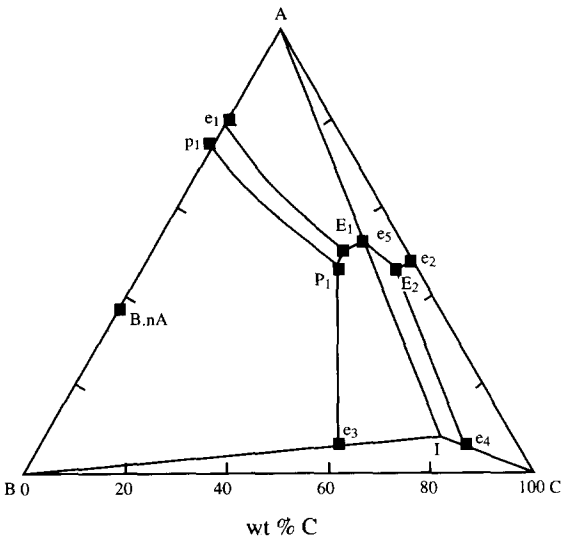

Fig. 7. General appearance of the phase diagram projection for a ternary system ABC with a ternary compound I and an incongruently melting hydrate $B \cdot nA$. Key: e_1 is eutectic $\langle A\rangle + \langle B \cdot xA\rangle + L/\langle A\rangle + \langle B \cdot nA\rangle$; p_1 is peritectic $\langle B \cdot nA\rangle + L/\langle B\rangle + L$; e_2 is eutectic $\langle A\rangle + \langle C\rangle + L/\langle A\rangle + \langle C\rangle$; e_3 is eutectic $\langle B\rangle + \langle I\rangle + L/\langle B\rangle + \langle I\rangle$; e_4 is eutectic $\langle I\rangle + \langle C\rangle + L/\langle I\rangle + \langle C\rangle$; e_5 is eutectic $\langle A\rangle + \langle I\rangle + L/\langle A\rangle + \langle I\rangle$; E_1 is ternary eutectic $\langle A\rangle + \langle B \cdot xA\rangle + \langle I\rangle + L/\langle A\rangle + \langle B \cdot nA\rangle + \langle I\rangle + L$; E_2 is ternary eutectic $\langle A\rangle + \langle I\rangle + \langle C\rangle + L/\langle A\rangle + \langle I\rangle + \langle C\rangle$; P_1 is ternary peritectic $\langle B \cdot nA\rangle + \langle I\rangle + L/\langle B\rangle + L$. L indicates unsaturated solution.

secondary crystallisation (incongruent melting) have common lines of intersection in three-dimensional space and can be represented by their projections on the composition triangle (for example, lines e_1E_1 and p_1P_1 in Fig. 7).

Secondary crystallisation surface of water + NaCl · 2H₂O. Secondary crystallisation temperatures of compositions belonging to the water crystallisation domain (compositions denoted by □, ● and ■ in Fig. 1) are independent of the water content but are functions of the ratio sucrose/NaCl. Eq. (2) gives the temperatures (T_3) of the ice + NaCl · $2H_2O$ secondary crystallisation, as a function of the sucrose/NaCl ratio R for the range $0 < R < 1.5$.

$$T_3 = -1.70R + 252 \tag{2}$$

with a standard deviation of 0.369, and a maximum of 0.617. Seven points from this work and two points from Ref. [10] were used for the construction of Eq. (2).

The coordinates of points belonging to the projection of this line on the composition triangle were determined analytically by the simultaneous solution of Eqs. (1) and (2). Points belonging to the monovariant line of the secondary crystallisation ice + NaCl · $2H_2O$ are marked in Fig. 9. The composition coordinates of these points were estimated by means of a short extrapolation. The errors in the concentrations shown as points on the monovariant line of secondary crystallisation are estimated as 1–2%.

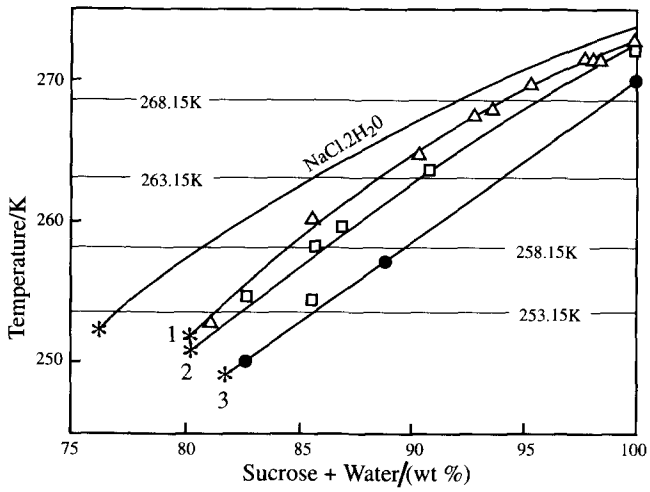

Fig. 8. Liquidus temperatures for isopleths 1–3 in Fig. 1. Curves 1, 2, 3 are NaCl sections at constant sucrose/NaCl ratio (Fig. 1); △, □, ●, experimental temperatures (T_4) from DSC curves; *, calculated points on the line of secondary crystallisation of $NaCl \cdot 2H_2O$ + ice (see text).

Secondary crystallisation surfaces of NaCl + IV and sucrose + IV. The points belonging to the projection of the lines of secondary crystallisation are marked in Fig. 9. The points from Ref. [9] were determined graphically from Fig. 1 in Ref. [9]; the errors are estimated as 1–2%. Temperatures of the secondary crystallisation of NaCl + IV as function of water/sucrose ratios are shown in Fig. 10 (line P_1F).

Four points for the temperatures T_s of the secondary crystallisation of sucrose + IV are obtained from Refs. [9] and [10] and are fitted by Eq. (3)

$$T_s = -152x^2 + 264x + 234 \tag{3}$$

with a standard deviation of 0.433, and a maximum deviation of 0.343; x is the water/NaCl mass ratio.

The incongruent melting surface of $NaCl \cdot 2H_2O$. This surface describes the incongruent melting of $NaCl \cdot 2H_2O$ in the ternary system. Melting temperatures as a function of the sucrose/water ratio are given in Fig. 10 (line p_1P_1). Note that in this ratio the water associated with $NaCl \cdot 2H_2O$ is not included. To construct the projection of the line of incongruent melting, the data from this work were

Table 2
Fitting parameters in Eq. (1)

Sucrose/water ratio	k	l	m	Standard deviation	Max. deviation
0.111	−29.7	5.46	−0.0244	0.354	0.596
0.25	123	1.99	−0.00497	1.23	1.86
0.424	143	1.43	−0.00158	0.00	0.00

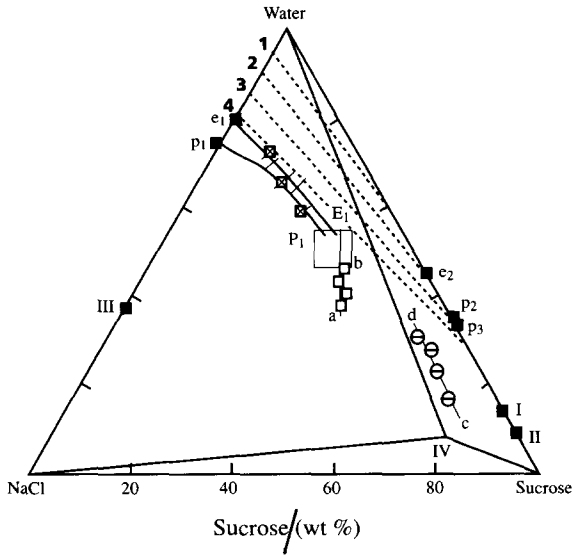

Fig. 9. Equilibrium phase diagram of the water–NaCl–sucrose system; for the general case, see Fig. 7. ⊠, points on the projection of the line of secondary crystallisation of $NaCl \cdot 2H_2O$ + ice; short bars: points on the line of incongruent melting of $NaCl \cdot 2H_2O$; the ternary peritectic point P_1 lies inside the square. e_1E_1 is the projection of the line of secondary crystallisation of $NaCl \cdot 2H_2O$; broken lines are water liquidus isotherms, determined graphically from Fig. 8 at 265.15 K, 258.15 K, 263.15 K, 268.15 K; for ab, cd lines, see Fig. 4; p_1, e_1 shows compositions of the eutectic and peritectic points for the NaCl–water system; e_2, p_2 and p_3 are shown in Fig. 3 and Table 1.

combined with results from Refs. [9] and [10]. Fig. 11 represents the polythermic $NaCl \cdot 2H_2O$ sections at a constant sucrose/H_2O ratio. The points shown on the solubility lines were estimated graphically from Fig. 4, with an estimated error of 2–3%. The lines pb and p′b′ are parallel to the composition line because the latter belongs to the linear surface of the incongruent melting of $NaCl \cdot 2H_2O$. The coordinates of the points on the projection of the line of incongruent melting (p_1P_1 in Fig. 7) were estimated as the intersection points of the lines pa and pb (p′a′ and p′b′). The estimated error of 4–5% includes the uncertainties of the points on the solubility lines and of the extrapolation. Note also the considerable disagreement between the solubility data reported in Refs. [9] and [10].

(3) Ternary peritectic points. It is now possible to arrive at a semi-quantitative estimate of the coordinates of the ternary peritectic point. This is the point of intersection of the lines of incongruent melting of the $NaCl \cdot 2H_2O$ (p_1P_1 in Fig. 7) and of the NaCl + IV secondary crystallisation (e_3P_1 in Fig. 7). Temperatures of the secondary crystallisation of NaCl + IV for compositions belonging to the crystallisation domain of NaCl (the BP_1e_3 field in Fig. 7) are functions of the sucrose/water ratio (Fig. 10). Similarly, the temperature of the incongruent melting of IV is a

function of the sucrose/water ratio (excluding water in the hydrate). The peritectic temperature and the sucrose/water ratio for the peritectic composition (P_1) have been estimated by extrapolation (Fig. 10) as 268.8 K and 0.7 respectively. The peritectic composition can also be estimated graphically from the composition triangle, by linear extrapolation of the projection of the line of secondary crystallisation NaCl + IV (ab) up to a sucrose/water ratio of 0.7. The approximate location of the ternary peritectic is marked in Fig. 9 by a square.

4. Conclusions

(1) Temperatures of ice melting and secondary melting of ice + $NaCl \cdot 2H_2O$ have been determined by DSC.

(2) The water-rich part of the equilibrium phase diagram wtih the water liquidus surface, the surface of secondary crystallisation of ice + $NaCl \cdot 2H_2O$ and the incongruent melting of $NaCl \cdot 2H_2O$ are represented as projections on the composition triangle.

(3) A semi-quantitative estimate of the coordinates of the ternary peritectic point has been made on the basis of our own and literature data.

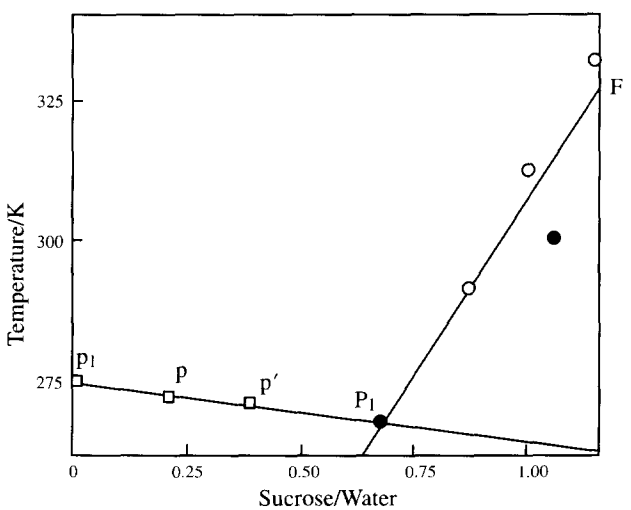

Fig. 10. Temperatures of the secondary crystallisation of NaCl + compound and the incongruent melting of $NaCl \cdot 2H_2O$ as a function of the sucrose/water ratio: ○, ●, points on the line of secondary crystallisation of NaCl + IV (from Refs. [8] and [9], respectively); □, points on the line of incongruent melting of $NaCl \cdot 2H_2O$, determined graphically from Fig. 11; P_1 peritectic point for the NaCl–water system. The lines were constructed by a least-squares linear regression. Lines P_1F and p_1P_1 show the relations between the sucrose/water ratio and the temperature of secondary crystallisation of NaCl + IV and the temperatures of incongruent melting of $NaCl \cdot 2H_2O$, respectively.

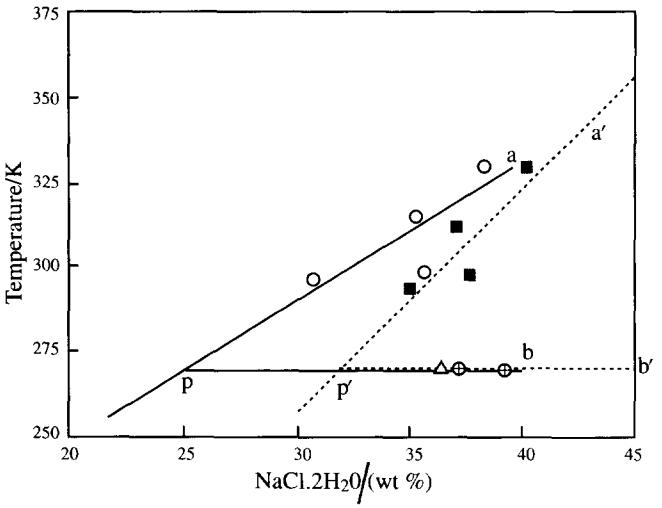

Fig. 11. Isoplethal section NaCl · $2H_2O$ for sucrose/water ratios of 0.355 and 0.191. ○, ■ are points belonging to the surface of NaCl solubility for sucrose/water ratios of 0.355 and 0.191, respectively, from Refs. [8] and [9]; △, ⊕: experimental points on the monovariant surface of the incongruent melting of NaCl · $2H_2O$ (T_1 endotherm on DSC curves) for sucrose/water ratios of 0.355 and 0.191, respectively. Lines pa and p'a' were constructed by a least-squares linear regression.

Acknowledgements

The authors express their gratitude to Ross Hatley, Barry Aldous, Tony Auffret and Patrick Echlin for constructive discussions. E.Yu. Shalaev also thanks the Royal Society for a Fellowship, the Fellows of Clare Hall, Cambridge, for a Visiting Associateship and Pafra Biopreservation for hospitality during his stay in the UK.

References

[1] (a) T. Suzuki and F. Franks, J. Chem. Soc. Faraday Trans., 89 (1993) 3283.
(b) M. Murase and F. Franks, Biophys. Chem., 34 (1989) 293.
[2] E.Yu. Shalaev, D.V. Malakhov, A.N. Kanev, V.I. Kosyakov, F.V. Tuzikov, N.A. Varaksin and V.I. Vavilin, Thermochim. Acta, 196 (1992) 213.
[3] A.N. Kanev, V.I. Kosyakov, D.V. Malakhov and E.Yu. Shalaev, Izv. Sib. Otd. Akad. Nauk SSSR, Ser. Khim. Nauk, 2 (1989) 11–15.
[4] R.H.M. Hatley, F. Franks and M. Green, Thermochim. Acta, 156 (1989) 247.
[5] D.A. Petrov, Zh. Fiz. Khim., 14 (1940) 1498 (in Russian).
[6] D.G. Archer, J. Phys. Chem. Ref. Data, 21 (1992) 793.
[7] F.E. Yong and F.T. Jones, J. Phys. Colloid Chem., 53 (1949) 1334.
[8] I.G. Druzhinin and S.A. Arbayev, Izv. Akad. Nauk Kirgiz. SSR, 2 (1960) 95.
[9] M. Schoorl, Rece. Trav. Chim. Pays-Bas, 42 (1923) 790.
[10] A.P. MacKenzie, Scanning Electron Microscopy, Part II, IIT Research Institute, Chicago, IL, 1972, p. 273.